

# Mass spectrometry of neutrals and positive ions in He/CO<sub>2</sub> non-equilibrium atmospheric plasma jet

Gert Willems<sup>1</sup>, Ante Hecimovic<sup>2,4</sup> , Kerstin Sgonina<sup>3</sup>,  
Emile Carbone<sup>2</sup>  and Jan Benedikt<sup>3</sup> 

<sup>1</sup> Research Department Plasmas with Complex Interactions, Ruhr-University Bochum, Bochum, Germany

<sup>2</sup> Max Planck Institute for Plasma Physics, Garching, Germany

<sup>3</sup> Institute of Experimental and Applied Physics, Kiel University, Kiel, Germany

E-mail: [ante.hecimovic@ipp.mpg.de](mailto:ante.hecimovic@ipp.mpg.de)

Received 31 July 2019, revised 14 December 2019

Accepted for publication 14 January 2020

Published 10 February 2020



## Abstract

Neutral species and positive ions are measured by means of mass spectrometry in the effluent of the non-equilibrium atmospheric plasma jet operated in He/0%–1%CO<sub>2</sub> gas mixture. The capacitively coupled plasma source is the predecessor of the known COST reference jet with identical performance and it is operated in a diffuse mode with gas temperature close to the room temperature. Threshold ionisation molecular beam mass spectrometry is used to measure absolute densities of CO, O<sub>2</sub>, O and O<sub>3</sub> species. The CO molecules are generated with densities up to  $2 \times 10^{15} \text{ cm}^{-3}$  at 1 W absorbed power. The O<sub>2</sub> density is  $\sim 6$  times lower than the CO density and even lower than the O density at level of  $4.5 \times 10^{14} \text{ cm}^{-3}$ . The O<sub>3</sub> density is negligibly small at  $4 \times 10^{12} \text{ cm}^{-3}$ . The measured O<sub>2</sub>, O<sub>3</sub> and O absolute densities add up to  $\sim 57\%$  of the expected oxygen amount. The high O density could indicate that the vibrational excitation of CO<sub>2</sub> is ineffective in this plasma and gas mixture, because O would otherwise react quickly with vibrationally excited CO<sub>2</sub>(v) to form CO and O<sub>2</sub>, the low energy efficiency is in agreement with the possibly low vibrational excitation. The highest energy efficiency is just 5% with 1% conversion efficiency. Ion mass spectrometry have been used to measure positive and negative ions, where only positive ions have been detected. The ion with highest signal is the O<sub>2</sub><sup>+</sup> ion, probably due to its low ionisation energy. CO<sub>2</sub><sup>+</sup>, O<sub>3</sub><sup>+</sup>, (CO)<sub>2</sub><sup>+</sup>, but no CO<sup>+</sup>, and protonated clusters or clusters containing water molecules have been detected as well. Neutrals and positive ions have been measured as a function of CO<sub>2</sub> admixture, applied power and distance to the jet nozzle. The observed trends can be used for validation of plasma-chemistry models.

Keywords: atmospheric plasmas, molecular beam mass spectrometry, CO<sub>2</sub> conversion

(Some figures may appear in colour only in the online journal)

## Motivation

Climate change and the influence of greenhouse gases, CO<sub>2</sub> in particular, has been high on the societal, political and economical agenda in the past years. This has lead to increasing efforts to find technical solutions. Among those is the idea of *conversion into value-added chemicals and fuels*. Taking CO<sub>2</sub> as example, the idea is to convert waste products (CO<sub>2</sub>) into new chemicals or fuels.

<sup>4</sup> Author to whom any correspondence should be addressed

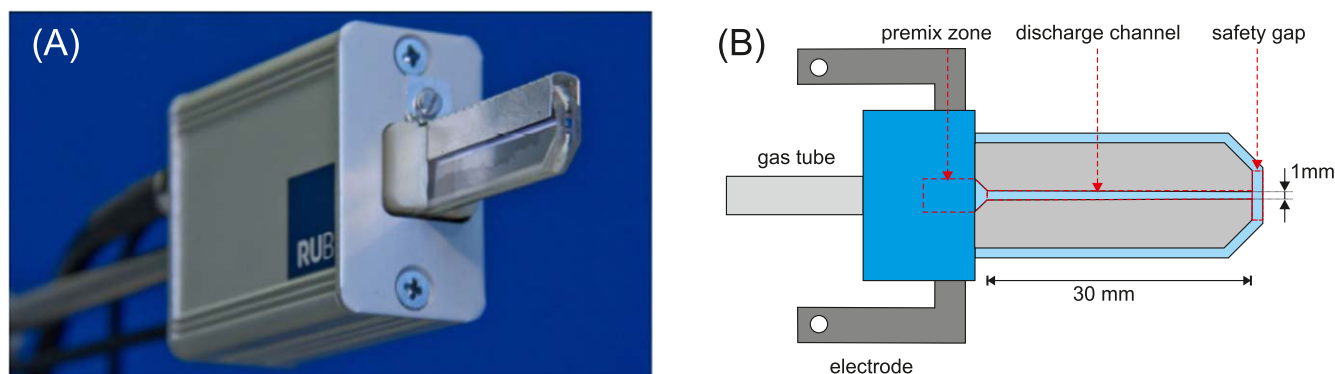


**Figure 1.** Picture (A) and illustration (B) of the COST reference jet. Two parallel electrodes are glued between two quartz glass plates with high-vacuum compatible glue. A detailed description can be found in [25]. Most of the experiments have been performed with external rf-power supply and match box, replacing the aluminum housing seen in the picture (A). Reproduced from [25]. © IOP Publishing Ltd. CC BY 3.0.

Emerging technologies, such as plasma-chemical conversion, focus on driving such conversion processes on the basis of sustainable energy sources, unlike traditional technologies that rely on heat provided by the burning of fossil fuels. Some noteworthy advantages of plasma-based technology are the low investment cost, the scalability, high throughput, no use of rare earth materials, and the gas activation by energetic electrons instead of heat [1]. The last point can be illustrated by pure  $\text{CO}_2$  splitting, which is briefly discussed here and treated in depth in literature [1, 2].

The dissociation of  $\text{CO}_2$  into the products CO and O requires breaking the C=O bond 5.5 eV. This can be achieved either by direct electron impact electronic excitation followed by dissociation which requires at least 7 eV, or by more energy efficient vibrational ladder climbing. The way to optimise the  $\text{CO}_2$  dissociation process through the vibrational ladder-climbing, it is needed to tune the electron energy distribution function in order to efficiently pump  $\text{CO}_2(v)$  molecules [3–5].

Atmospheric pressure plasmas can play a role in this field as they enable non-equilibrium chemistry and are easy to integrate in chemical installations. Several plasma sources are currently under investigation, often approached from the application point of view of high energy and conversion efficiency. The modelling efforts have either used a global models [6–11] or they were focused on various types of plasma discharges: dielectric barrier discharges (DBD) [12–14], microwave plasma (MW) [15–17], ns pulsed discharges [18], or gliding arc [19].

The focus of current kinetic modelling is on correct description of the  $\text{CO}_2$  vibrational state distribution [3, 4, 7] and the influence of vibrational–vibrational relaxation (V–V) and vibrational-translational relaxation (V–T) in collisions with electrons and heavy particles. Another approach is a  $\text{CO}_2$  plasma chemistry model by Koelman *et al* [8] using the PLASIMO code [20]. For all these models the knowledge of complete set of heavy particles and their absolute densities is of large importance. Such set should include the ground state molecules and atoms, vibrationally and rotationally excited molecules, and ions. In this work we present our contribution by providing information on density of ground state molecules and atoms, and presence of ions in the effluent of He/ $\text{CO}_2$  micro atmospheric pressure plasma jet. Commonly,

in the field of  $\text{CO}_2$  conversion using plasmas, the mass spectrometer is used as a tool for sampling of the cold gas mixture to determine the conversion of the given plasma process. In this paper we use an experimental approach in the subject of  $\text{CO}_2$  conversion where the molecular beam mass spectrometer is used to investigate kinetic of  $\text{CO}_2$  conversion through analysis of reactive O atoms and  $\text{O}_2$ , CO and  $\text{O}_3$  stable species which could be relevant and employed in future for the effluents of other discharge types.

The results presented here could also be used in the field of the low temperature plasma medical treatment which has gained a lot of attention as a promising therapy for wound and skin treatment [2, 21]. Additionally, low doses of CO shows therapeutic effects [22] and here studied plasma jet could be used in future medical treatments.

## Experimental setup

### Plasma source

Within the atmospheric pressure plasma research community, a reference plasma source has been developed in the framework of the COST (European COoperation in Science and Technology) Action M1101 ‘Biomedical Applications of Atmospheric Pressure Plasmas’. The COST reference jet is the latest step in the development of the ‘Atmospheric Pressure Plasma Jet’ that was initiated by Selwyn and co-workers [23, 24] and is known in previous versions as the  $\mu\text{APPJ}$ . Both the final version as well as earlier adaptations of it were used in the research presented here. The COST reference jet, illustrated in figure 1, is described in detail elsewhere [25] and here only a brief summary is given. It is a capacitively coupled atmospheric plasma jet, composed of two parallel electrodes glued between two quartz glass plates. It is glued with high-vacuum compatible glue, which reduces impurity intrusion significantly. The electrodes are 1 mm thick and 30 mm long and are placed at 1 mm distance from each other. The plasma jet is operated at 13.56 MHz and typically a voltage of 200 to 230  $V_{\text{RMS}}$  is applied. The absorbed power is usually below 2 W. When operated in Helium (5.0 purity)

with small admixture of molecular gases ( $<1.5\%$ ), the plasma jet operates in a homogeneous alpha-mode (glow discharge) with electron densities of approximately  $1 \times 10^{11} \text{ cm}^{-3}$  [26]. The applied helium flow is always 1.4 slm.

Without any changes to the set-up, it is not possible to surround the COST reference jet completely with a protective He atmosphere, as parasitic plasmas ignite in the jet's housing. Therefore, here presented measurements were conducted using a variant of the COST reference jet, called here the MS (mass spectrometer) variant jet. The design of the MS variant jet is in essence identical to the COST reference jet. The sole difference is the use of an external, not built-in, power supply, impedance matching network and voltage probe. Furthermore, no current probe was used. Due to this difference, the ignition of parasitic plasmas is avoided. The use of an external power supply does not change the plasma itself since its properties are determined by the applied voltage waveform.

As no current probe was used, the delivered power cannot be calculated for the MS variant jet, in contrast with the COST reference jet. Therefore, the voltage was fixed throughout experiments instead of power. It is shown in literature that this has an influence on the density of produced species when varying the admixture of additional gases [25], since the absorbed power by the plasma decreases with an increasing admixture. It is paramount to keep this in mind when comparing experiments by MS (using the MS variant jet) with other experiments (using the COST reference jet) or plasma models, where not the applied voltage, but the absorbed plasma power is kept constant. Experiments with the COST reference jet were conducted under the same experimental conditions and compared with the MS variant jet results for several gas mixtures ( $\text{He}/\text{H}_2\text{O}$ ,  $\text{He}/\text{N}_2/\text{O}_2$  and  $\text{He}/\text{O}_2$ , see for example [27, 28]) with excellent agreement among measured densities.

#### Details of mass spectrometry measurements

In this work two molecular beam mass spectrometers were used. Each mass spectrometer comprise of particular design and each MS is incorporated in a different experimental setup. One has been built to measure neutral species and the other to measure charged species. The particular details of each MS have been discussed at length in previous publications given below and the discussion is limited here, therefore, just to the essentials of both systems. For the reason that neutral and ion measurement are done at different setups, there are small differences between the measurement positions and conditions for the two experiments.

**Mass spectrometry of neutral species.** The mass spectrometer for neutral species, further abbreviated to NMBMS (neutral molecular beam mass spectrometer), was the main diagnostic. The development and design of this system is described in our earlier work [29–31]. Since then, some changes occurred and upgrades were added, which are shortly described here. From the set-up, the actual mass spectrometer elements: quadrupole, SEM (secondary electron multiplier) and detector have been changed. Earlier a HIDEN™ Hal 4 PSM QMS system had been used, which has been replaced by a Pfeiffer™ HiQuad QMG700 (mass

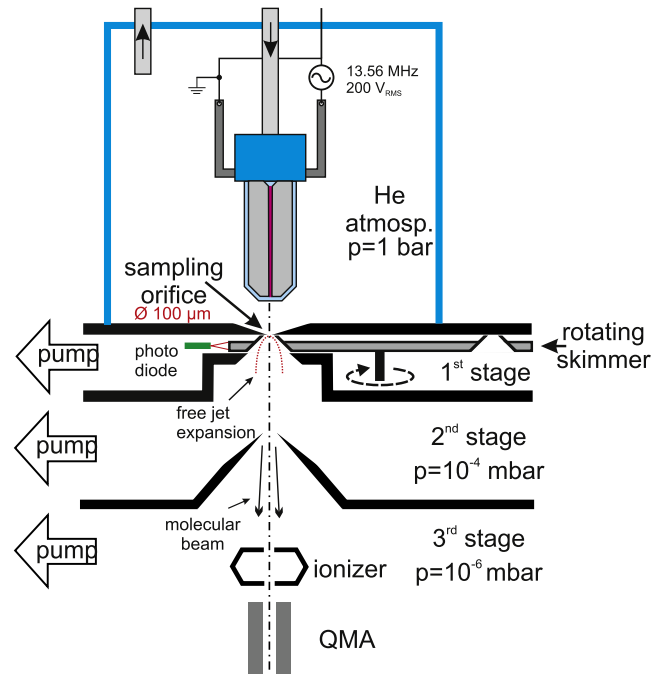


**Figure 2.** Schematic of the mass spectrometer to measure neutral species. The effluent is sampled into a triple staged differentially pumped system. A rotating skimmer/chopper fulfills two roles: correcting for background signal and stopping gas flow into 2nd and 3rd stage. As a result, a very high signal-to-background ratio is achieved.

range: 0–2400 u). This system is equipped with an electron impact ionisation source and a discrete secondary electron multiplier (SEM). The plexiglas® cylinder used to create the protective atmosphere has been upgraded to a full glass cylinder, with a larger volume of 8.5 L. A cold trap was added to the last differential pumping stage, where the mass spectrometer is installed, with the main aim of reducing the water vapour background pressure.

The mass spectrometer is schematically presented in figure 2. The effluent of the plasma jet is sampled through a  $\varnothing = 100 \mu\text{m}$  orifice into a differentially pumped system. It should be kept in mind that the central axis of the plasma jet is aligned with this orifice, therefore effects of radial diffusion can appear for reactive species. The relatively large orifice diameter is possible because the applied electric field is confined between the electrodes of the plasma jet. The plasma is not in direct contact with the sampling orifice and there is no danger of electric-field-penetration into the low pressure part of the pumping stage, where it could otherwise ignite a parasitic plasma. A molecular beam is formed from the sampled gas and passes through the ioniser of the quadrupole mass spectrometer in the third stage, where the electron impact ionisation takes place.

A specially designed chopper with rotating skimmer is installed just behind the (first) sampling orifice. It fulfills two roles: allowing the correction for the signal due to background gas in the ionizer and being a valve between the first and second/third stage. The latter allows for a significant reduction of background signal, resulting in a very high beam-to-background ratio [29]. Correction for background

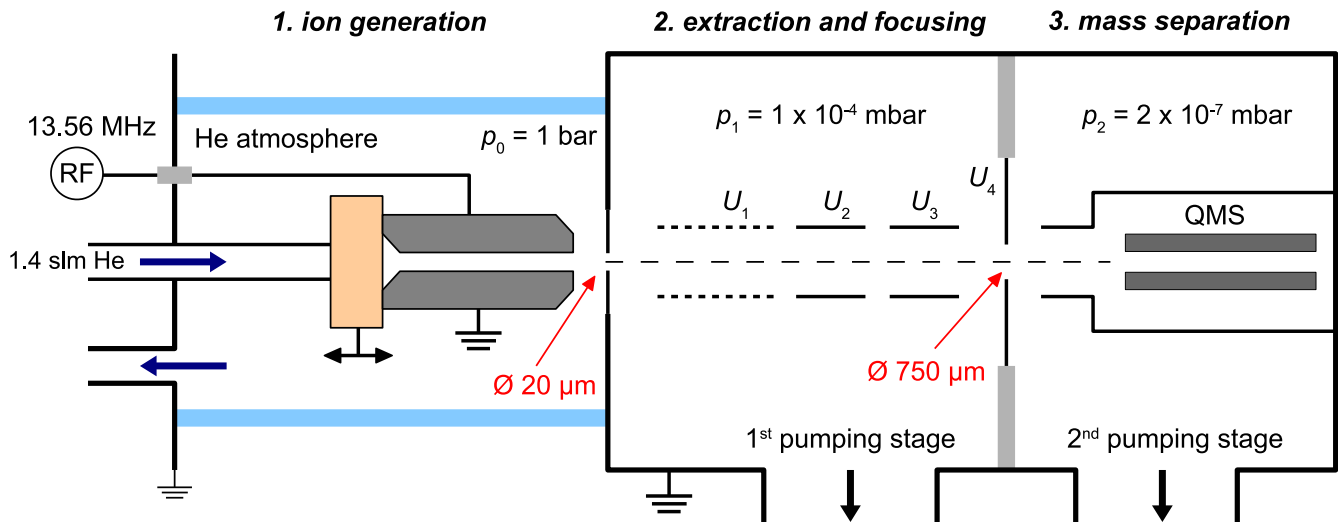


**Figure 3.** Schematic of the mass spectrometer to measure charged species. Ions are sampled into a two staged differentially pumped system. They are guided by electron lenses (U1–U4). Reproduced with permission from [36].

gas is possible because during one chopper rotation, the chopper is most of the time (98.5%) blocking the molecular beam. Hence, the ions arriving on the detector mainly originate from the background gas present in the mass spectrometer. Only during four brief time intervals ( $250 \mu\text{s}$ ), when one of the four skimmers is aligned with the sampling orifice, the gas from the atmospheric side is allowed to enter the system. By comparing signals at chopper open and chopper closed positions the signal originating from the sampled gas in the molecular beam can be calculated.

A gas flow that is directed towards a solid surface creates a stagnation zone in front of that solid surface. This applies here as the plasma jet effluent is sampled. The stagnation zone is  $100 \mu\text{m}$  under standard operating conditions (1.4 slm helium flow), as calculated by fluid modelling [32]. As the helium flow remains laminar, the gas in front of the mass spectrometer plate is pushed side-wards with respect to the orifice. Moreover, the design of the mass spectrometer ensures that no stagnation directly in front of the orifice takes place. Continuum collisional flow occurs ( $K_n \ll 1$ ) and gas species are accelerated into the sampling orifice. The sampling of gas species occurs at a height of  $200\text{--}500 \mu\text{m}$  above the orifice (2–5 times the diameter of the sampling orifice [33, 34]). After passing the sampling orifice the gas density in the molecular beam decreases steeply and the gas transport turns quickly into a molecular flow. Therefore, the reaction chemistry inside the sampled molecular beam is not affected and the gas composition gets frozen.

Absolute densities of reactive species can be determined with the help of a calibration gas with a known density that is admixed into the helium flow under the same experimental conditions. The unknown density of measured species is determined from the ratios of the mass-dependent transmission function of the mass spectrometer, measured signals, ionisation cross-sections and density of the calibration gas. The general calibration procedure is discussed in more detail in our other publications [35]. Here,  $\text{CO}_2$  and  $\text{O}_2$  densities have been calibrated directly with those stable species and the

$\text{CO}$ ,  $\text{O}$ , and  $\text{O}_3$  densities have been calibrated with  $\text{O}_2$ ,  $\text{Ne}$ , and  $\text{Ar}$ , respectively.

**Mass spectrometry of charged species.** The mass spectrometer for charged species is the same as designed and developed by Große-Kreul [36] and is illustrated in figure 3. Again, the effluent of the plasma jet is sampled into a differentially pumped system consisting of two pumping stages. This time, the sampling orifice is smaller,  $\varnothing = 20 \mu\text{m}$ . A set of ion lenses is used to extract and guide ions to the Besselbox filter of the quadrupole mass spectrometer. The ion lenses settings are mass dependent, which should be taken into consideration [37]. The mass spectrometer is equipped with a channeltron SEM. The QMA mass range is up to  $300 \text{ amu}$  and the Besselbox energy range is  $-100$  to  $+100 \text{ eV}$ . An electron impact ionisation source is present, but not used when measuring ions. No beam chopper is required for ion measurement.

The ion energy distribution function (IEDF) can be measured. For atmospheric pressure plasma jets this generally does not provide much new insights (all the ions are thermalised due to high collision frequency), so the IEDF is mainly measured to ensure that charged species originate from atmospheric pressure and no secondary, parasitic plasma is generated inside the vacuum chamber. An absolute density calibration of the mass spectrometer is unfortunately not possible. The measured signal can be correlated with the density of charged species using an extended ion transport model [37], but it was not performed here and only relative signal intensities as function of mass and distance to the jet nozzle are presented and an order of magnitude estimation is made.

As discussed by Große-Kreul, the mass spectrometer settings of energy, cylinder and endcap are mass dependent [37]. The relation for energy at a fixed value of cylinder and endcap is  $E_{\text{kin}}(\text{eV}) = ((1.2 \pm 0.1) \times 10^{-2}) m (\text{amu})$ .



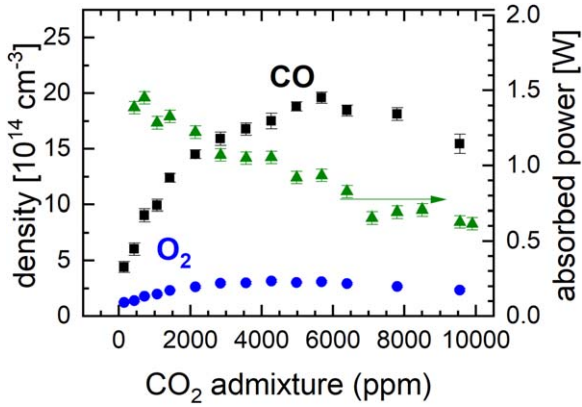


**Figure 4.** Density of CO and O<sub>2</sub> and the power absorbed by plasma as a function of CO<sub>2</sub> admixture. The distance was 4 mm and applied voltage 230 V<sub>RMS</sub>.

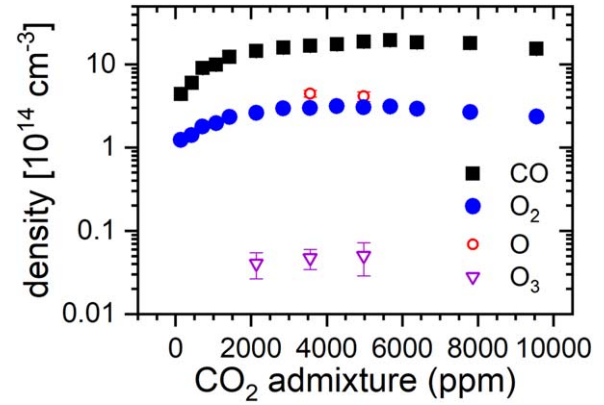


**Figure 5.** Density of CO, O<sub>2</sub>, O, and O<sub>3</sub> as a function of CO<sub>2</sub> admixture. The distance was 4 mm and applied voltage 230 V<sub>RMS</sub>.

## Experimental results and discussion

### Absolute densities of neutral species

The absolute densities of CO and O<sub>2</sub> as function of CO<sub>2</sub> admixture are presented in figure 4. The measurements were made at 4 mm distance from the electrodes and 230 V<sub>RMS</sub> applied voltage. The trend appears to be the same for both CO and O<sub>2</sub>: an initial increase in density culminates in a maximum around 5500 ppm and is then followed by a decrease, which can be explained by the decrease of the measured absorbed power. The CO density is about 6 times higher than the O<sub>2</sub> density. Additionally, the CO<sub>2</sub> density has been measured in the gas mixture (plasma off) and with plasma turned on. The difference of these two densities provide the information about CO<sub>2</sub> consumption. However, this consumption is, as we will discuss later, small and the subtraction of the two large numbers results in scattered data and is, therefore, not shown here.

The performance of the jet is determined by its geometry, gas flow and gas mixture and the applied root-mean-square voltage independent of the power supply used due to very small current (absorbed power below 1 W). The absorbed power plotted in figure 4 was measured for COST jet where measurements of both current and voltage are possible. For the jets used in the here presented experiments only voltage is measured. The data plotted in figure 4 are for the COST jet at the same conditions. Based on our experience the values of the current and the voltage are comparable between the jets within accuracy of 10%.

The error bars given for each data point in figure 4 are derived from the statistical distribution of the measured signals and calibration measurements performed.

The ratio of CO versus O<sub>2</sub> is expected to be two, based on the overall reaction  $2\text{CO}_2 \rightarrow 2\text{CO} + \text{O}_2$ . Since the measured ratio is around 6, the measured products are deficient in oxygen, accounting for only 34% of the expected amount. The most likely explanation of this discrepancy is that other oxygen containing molecules were not measured. Therefore, O and O<sub>3</sub> species were detected and calibrated in a new measurement campaign. However only a few data points could be measured due to long measurement times needed,

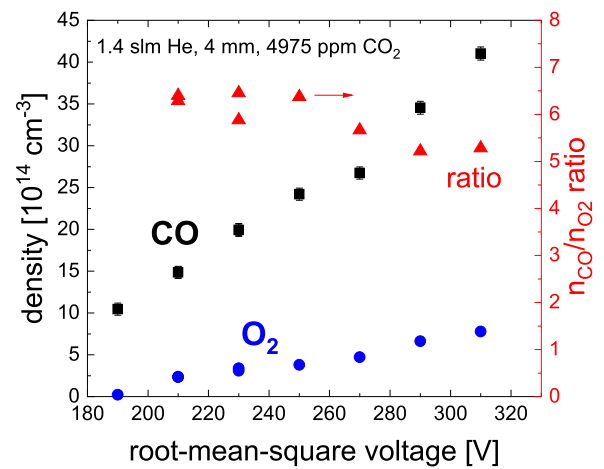


**Figure 6.** Density of CO (black) and O<sub>2</sub> (blue) and their ratio (red) as a function of applied voltage at 4 mm distance to the jet electrodes and 4975 ppm CO<sub>2</sub> admixture.

and no trends are, therefore, presented for their densities, see the results in figure 5.

The O density is 1.5 times higher than the O<sub>2</sub> density and about 100 times higher than the O<sub>3</sub> density. The high O density can be explained by its low reactivity towards ground state CO<sub>2</sub> ( $k \sim 1.2 \times 10^{-49} \text{ cm}^3 \text{ s}^{-1}$  [38]) and three body recombination of O with ground state CO (50 times slower than O<sub>2</sub> + O three body recombination [38, 39]). The low density of O<sub>2</sub> is also responsible for the low loss of O in the three body recombination with O<sub>2</sub> to O<sub>3</sub>, which also explains the low measured O<sub>3</sub> density. The sum of O<sub>2</sub>, O<sub>3</sub> and O species account now for 57% of the expected oxygen. It is not clear at the moment, whether the remaining deficiency of the gas mixture in oxygen is due to loss of oxygen in reactions with gas impurities (mainly N<sub>2</sub>, H<sub>2</sub>O leading to NO<sub>x</sub> or H<sub>2</sub>O<sub>2</sub> species), surface reactions or due to possible systematic error in the density calibration.

The dependence of density of CO and O<sub>2</sub> species has been measured as the function of applied voltage (Figure 6) and distance to the jet (figure 7) as well. Here, 4975 ppm CO<sub>2</sub> was admixed and the distance was kept at 4 mm and the applied voltage at 310 V<sub>RMS</sub>, respectively.

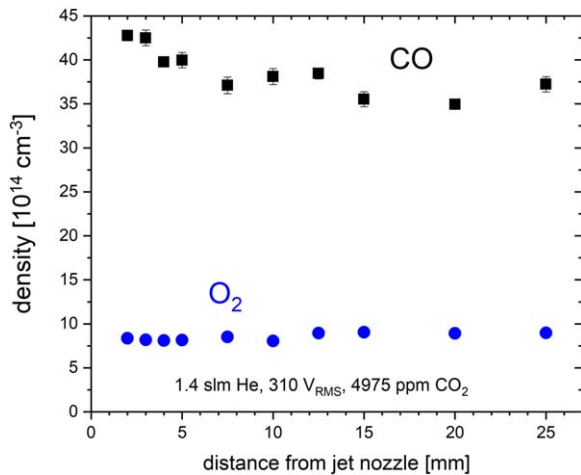


**Figure 7.** Density of CO (black) and O<sub>2</sub> (blue) as a function of distance to the jet electrodes at fixed 4975 ppm CO<sub>2</sub> admixture and 310 V<sub>RMS</sub> applied voltage, the parameters for which maximum signal of CO and O<sub>2</sub> was observed.

The density of both CO and O<sub>2</sub> increases linearly, while keeping a near constant ratio slightly decreasing towards 5 with increasing voltage. The density increase can be explained by an increase of input power that enhances the CO<sub>2</sub> dissociation in the plasma. It should be noted that applied voltage is not linearly proportional to input power as shown by Golda *et al* [25]. Both CO and O<sub>2</sub> species show constant densities during the distance variation, confirming them to be a final unreactive products of the plasma chemistry. The density of CO appears to drop ~20% in the first 4–5 mm and we discuss the possible reactions in the following.

The most common neutral–neutral species reactions used in CO<sub>2</sub> plasma modelling are given in table 1. The reaction rate constants were evaluated in case of three-body reactions with the density of He, the most abundant species, but it should be noted that only data for nitrogen as third body are provided in the literature.

Atomic oxygen transforms into O<sub>2</sub>, through a combination of reactions R01 and R05 in the effluent or by reaction R02 in the plasma. No rate constant was found for the latter, but according to literature it is even faster than R01 [2]. Reaction R02 is also essential to make the CO<sub>2</sub> conversion energy efficient by removing atomic oxygen. The main O<sub>2</sub> loss reaction here, R03, is compensated by production reaction R01, explaining the constant O<sub>2</sub> density as a function of distance.

The ozone density is governed by reactions R03–R05 and R15. As R03 is faster than the other reactions, the balance is tilted towards production of ozone by three-body recombination. Therefore, it is expected that the trend of ozone density as a function of distance will be a linear increase until O is consumed. The trend as a function of admixture is more uncertain, it most likely will follow a combined trend of O and O<sub>2</sub>.

All production reactions of CO (R06–R12) are very slow. For reactions R08–R10, the density of C is unknown. Based

on discussions about CO<sub>2</sub> modelling [42], the density is estimated to be at the very maximum  $1 \times 10^{10} \text{ cm}^{-3}$ . In fact, the density of C would have to be higher than the CO density to explain the measurements. Likewise, for reactions R11–R12, the density of C<sub>2</sub>O is unknown. C<sub>2</sub>O is usually not taken into consideration in CO<sub>2</sub> models, because of its significantly lower density. The slow reactions explain why the CO density does not increase with distance in the effluent. This also implies that the increase of CO density with increasing precursor admixture must originate from inside the plasma region. However, the reaction chemistry inside the plasma region is out of the scope of this work.

The observed small decrease of the CO density in the first millimetres of the distance variation (figure 7) cannot be fully explained on the basis of the available reactions. It would require an effective rate of  $3.50 \pm 0.56 \times 10^{18} \text{ cm}^{-3} \text{ s}^{-1}$  as estimated based on the density decrease and gas velocity of  $20 \text{ m s}^{-1}$ . None of the loss reactions listed above is fast enough. Reaction R13 is a factor  $10^4$  too slow, reactions R14 and R15 a factor  $10^{33}$  and  $10^{15}$  respectively (using the measured or known densities to calculate the rates) and reaction R16 would require the density of C to be equal to the one of CO. Assuming that there are 5 O(<sup>1</sup>D) atoms per 100 O atoms, reaction R17 would be fast enough. However, CO reacts effectively with O(<sup>1</sup>D) and therefore the maximum decrease of CO is limited by the O(<sup>1</sup>D) density. Even if all the O would be O(<sup>1</sup>D), it still cannot explain the observed decrease. Reaction R18 follows a similar argument, but is under all assumptions too slow. Reactions of CO with N<sub>2</sub> and H<sub>2</sub>O as 5 ppm and 2 ppm impurity, respectively, in the helium feed gas, originating from the gas bottle, were also considered. Radial diffusion is another possible explanation, although unlikely. The diffusion effect would be present for the complete measured distance range (=up to 25 mm) and not only the first millimetres, furthermore it would manifest itself for O<sub>2</sub> as well.

Another possible explanation is the presence of CO by dissociative ionisation of vibrational excited CO<sub>2</sub>. CO is measured with an electron energy of 18 eV to avoid dissociative ionisation of CO<sub>2</sub>. Vibrationally excited CO<sub>2</sub> (CO<sub>2</sub>(v)), however, has a lower ionisation threshold and subsequently a lower threshold for dissociative ionisation. Considering that CO<sub>2</sub>(v) is still present in the effluent just behind the jet nozzle and it is quenched within few millimetres, it could explain the extra CO signal that is observed the first millimetres of the effluent. The presence of CO<sub>2</sub>(v) in the effluent can be verified by a measurement of CO<sub>2</sub>, while varying the electron energy in the ionizer and keeping all other experimental parameters constant. Such a measurement was conducted during the experimental campaign at the distance of 4 mm and no CO<sub>2</sub>(v) could be detected (signal under ionisation threshold of ground state CO<sub>2</sub>) in the effluent. Therefore, we do not have any reasonable explanation for the CO density decrease in the distance measurement. It should be noted that the CO<sub>2</sub>(v) can still be present in the active plasma zone between the electrodes.

**Table 1.** Reactions used in the discussion of most likely production and loss reactions in the effluent of a plasma in a He/CO<sub>2</sub> gas mixture. The reaction rate coefficients are evaluated at  $T = 315$  K.

	Reactants	Products	$k(\text{cm}^3 \text{s}^{-1})$	References
R01	O + O + M	O <sub>2</sub> + M	$2.11 \times 10^{-14}$	<sup>a</sup> [8]
R02	O + CO <sub>2</sub> *	O <sub>2</sub> + CO		[2]
R03	O + O <sub>2</sub> + M	O <sub>3</sub> + M	$7.47 \times 10^{-15}$	<sup>a</sup> [40]
R04	O <sub>3</sub> + M	O <sub>2</sub> + O + M	$1.67 \times 10^{-06}$	<sup>a,b</sup> [8]
R05	O + O <sub>3</sub>	O <sub>2</sub> + O <sub>2</sub>	$1.17 \times 10^{-14}$	[40]
R06	CO <sub>2</sub> + M	CO + O + M	$1.17 \times 10^{-58}$	<sup>a,b</sup> [8]
R07	CO <sub>2</sub> + O	CO + O <sub>2</sub>	$8.15 \times 10^{-48}$	[8]
R08	CO <sub>2</sub> + C	CO + CO	$1.00 \times 10^{-15}$	[8]
R09	O <sub>2</sub> + C	CO + O	$3.00 \times 10^{-11}$	[38]
R10	O + C + M	CO + M	$5.22 \times 10^{-13}$	<sup>a</sup> [8]
R11	O + C <sub>2</sub> O	CO + CO	$9.51 \times 10^{-11}$	[8]
R12	O <sub>2</sub> + C <sub>2</sub> O	CO + CO <sub>2</sub>	$3.30 \times 10^{-13}$	[8]
R13	CO + O + M	CO <sub>2</sub> + M	$3.28 \times 10^{-16}$	<sup>a</sup> [8]
R14	CO + O <sub>2</sub>	CO <sub>2</sub> + O	$3.42 \times 10^{-45}$	[8]
R15	CO + O <sub>3</sub>	CO <sub>2</sub> + O <sub>2</sub>	$4.00 \times 10^{-25}$	[8]
R16	C + CO + M	C <sub>2</sub> O + M	$1.47 \times 10^{-12}$	<sup>a</sup> [8]
R17	CO + O( <sup>1</sup> D)	CO <sub>2</sub>	$8.00 \times 10^{-11}$	[8]
R18	O <sub>2</sub> (b <sup>1</sup> $\sigma_g^+$ ) + CO	Products	$3.74 \times 10^{-15}$	[41]

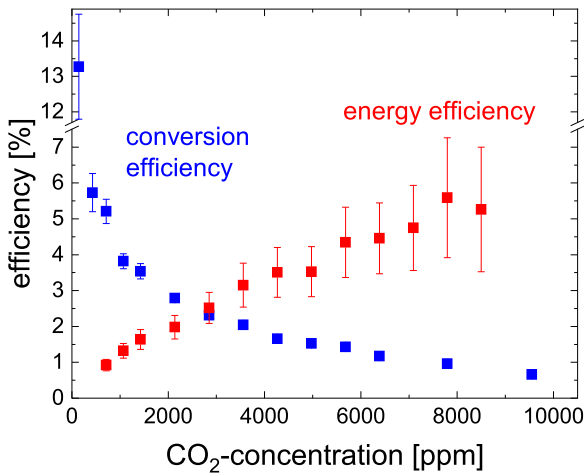
<sup>a</sup>  $k$  of three-body reaction is already multiplied by  $n_{\text{He}}$ .<sup>b</sup>  $k$  has as unit:  $\text{k}(\text{s}^{-1})$ .**Figure 8.** Conversion and energy efficiency as function of CO<sub>2</sub> admixture, measurements are done at 4 mm.

Figure 8 shows the CO<sub>2</sub> conversion efficiency  $\eta_c$  and the net energy efficiency  $\eta_e$  calculated as:

$$\eta_c = \frac{n_{\text{CO}}}{n_{\text{CO}_2, \text{off}}}, \quad (1)$$

$$\eta_e = \frac{\Phi(n_{\text{CO}}) \cdot E_{\text{bond}}}{P_{\text{plasma}}}, \quad (2)$$

respectively, where  $n_{\text{CO}_2, \text{off}}$  is the CO<sub>2</sub> density without plasma,  $\Phi(n_{\text{CO}})$  is the flow of CO molecules at the jet exit,  $E_{\text{bond}}$  is the CO bonding energy in CO<sub>2</sub> molecule and  $P_{\text{plasma}}$  is the power absorbed by plasma as shown in figure 4.

The overview of conversion and energy efficiency obtained at different plasma sources for CO<sub>2</sub> conversion has been given by Snoeckx *et al* [1]. The highest achieved values are obtained using the microwave and RF plasmas;

conversion up to 90% at energy efficiency of up to 40%, and energy efficiency up to 90% at conversion efficiency up to 40%. The conversion and energy efficiency of a gliding arc was up to 20% and 70%, respectively. The DBD discharges have conversion and energy efficiency up to 40% and 15%, respectively. First it is important to mention that reported energy efficiency of 90% in the microwave discharge has been reported in 1980s, and have not been successfully reproduced since then. Secondly, for all plasmas it has been observed that the conversion and energy efficiency exhibit anti-correlation, indicating that simultaneous high conversion and high energy efficiency is not possible. For case of microwave plasmas, van den Bekerom *et al* argued that most of the currently achieved results can be explained by inhomogeneous heating with gas being in the thermal equilibrium [43].

Both efficiencies are in agreement with current understanding of CO<sub>2</sub> conversion. Higher conversion efficiency is achieved in the parameter range with high applied power per CO<sub>2</sub> molecule and low energy efficiency. On the contrary, the increasing energy efficiency is achieved with increasing CO<sub>2</sub> admixture, where, however, the conversion efficiency decreases below 1%. Both efficiencies are low, being more comparable to values obtained in DBD discharges [1] then compared to RF discharges where conversion of 80% have been reported [44–46]. The difference between here presented results is that the COST jet was operated in He/CO<sub>2</sub> gas mixture at atmospheric pressure, while in other experiments it was a pure CO<sub>2</sub> gas and the pressure was up to 40 Pa. The difference can be explained by high He dilution and low gas temperature. It could indicate an inefficient vibrational excitation preventing reaction R2 to be effective, which would also results in the observed high atomic oxygen density.

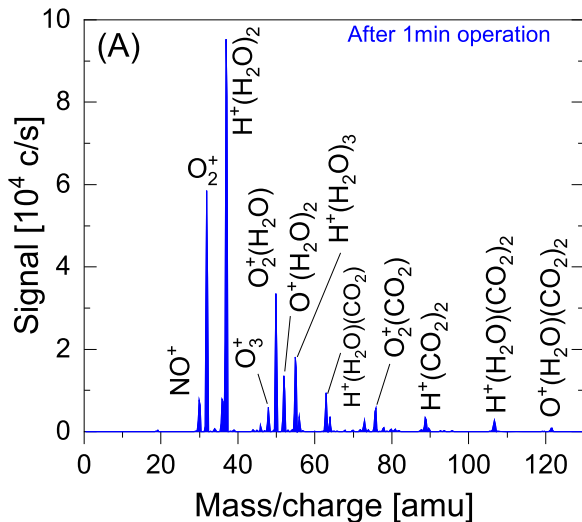


**Figure 9.** Ion mass spectrum of the plasma effluent in a He/CO<sub>2</sub> gas mixture immediately (1 min) after plasma ignition. The spectrum is dominated by protonated water clusters due to impurities in the set-up.

Higher conversion efficiencies can be achieved with more applied power into the discharge [47].

#### Relative measurement of charged species

The ion chemistry of an atmospheric pressure plasma is quite different from the ion chemistry of a low pressure plasma. Charged species produced in the plasma region in electron impact ionisation or Penning ionisation processes (we will call them in the following text primary ions) will, due to the very high collisional rate at atmospheric pressure, quickly undergo charge transfer reactions with neutral species inside the effluent. Ions with lower ionisation energy, including ion clusters, are favoured as most stable reaction products [48, 49].

The primary ion composition of an atmospheric pressure plasma, i.e. the composition in the plasma region, is thus modified. Next to a few primary ions, mainly secondary ions can be observed. These secondary ions are created by charge or proton transfer reactions as well as cluster formation reactions, e.g. the  $H^+(H_2O)_n$  cluster. Generally, such reactions dominate the ion chemistry in the plasma effluent (see for example [50, 51]).

The measurements of charged species in the effluent of the He/CO<sub>2</sub> plasma by means of ion mass spectrometry are presented and discussed here. Only positive ions in the plasma effluent could be detected since negative ions recombine quickly in the effluent and can only be observed when the sampling orifice is in contact with the active plasma [50]. Gas impurities present in the set-up after plasma ignition have a strong effect on the ion spectrum presented in figure 9. This effect is discussed in literature on the example of helium and He/N<sub>2</sub> plasma [52]. Immediately after plasma ignition, the ion spectrum is dominated by protonated water clusters  $H^+(H_2O)_n$ . The effect of impurities disappears after a certain waiting period, typically 30–60 min, and the measurements

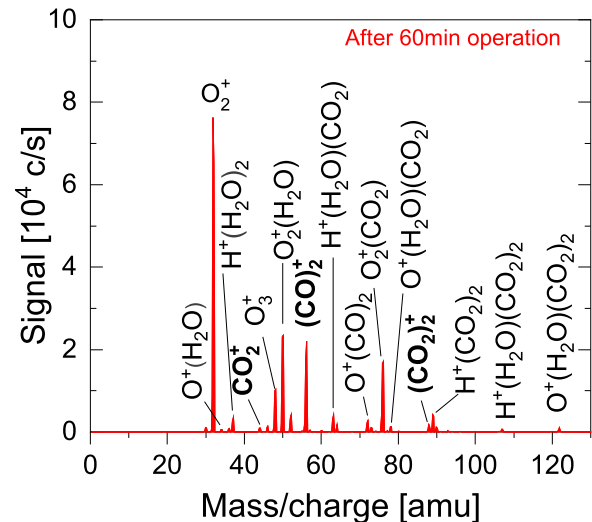


**Figure 10.** Ion mass spectrum of the plasma effluent in a He/CO<sub>2</sub> gas mixture after 60 min of operation.

with impurity level given by the gas purity in the feed gas, can be conducted. The assignment of ions to the measured masses is based on the most probable ion due to admixed gas. However, it cannot be excluded that other ions are also contributing. This is especially valid when a lot of impurities are present, as in figure 9.

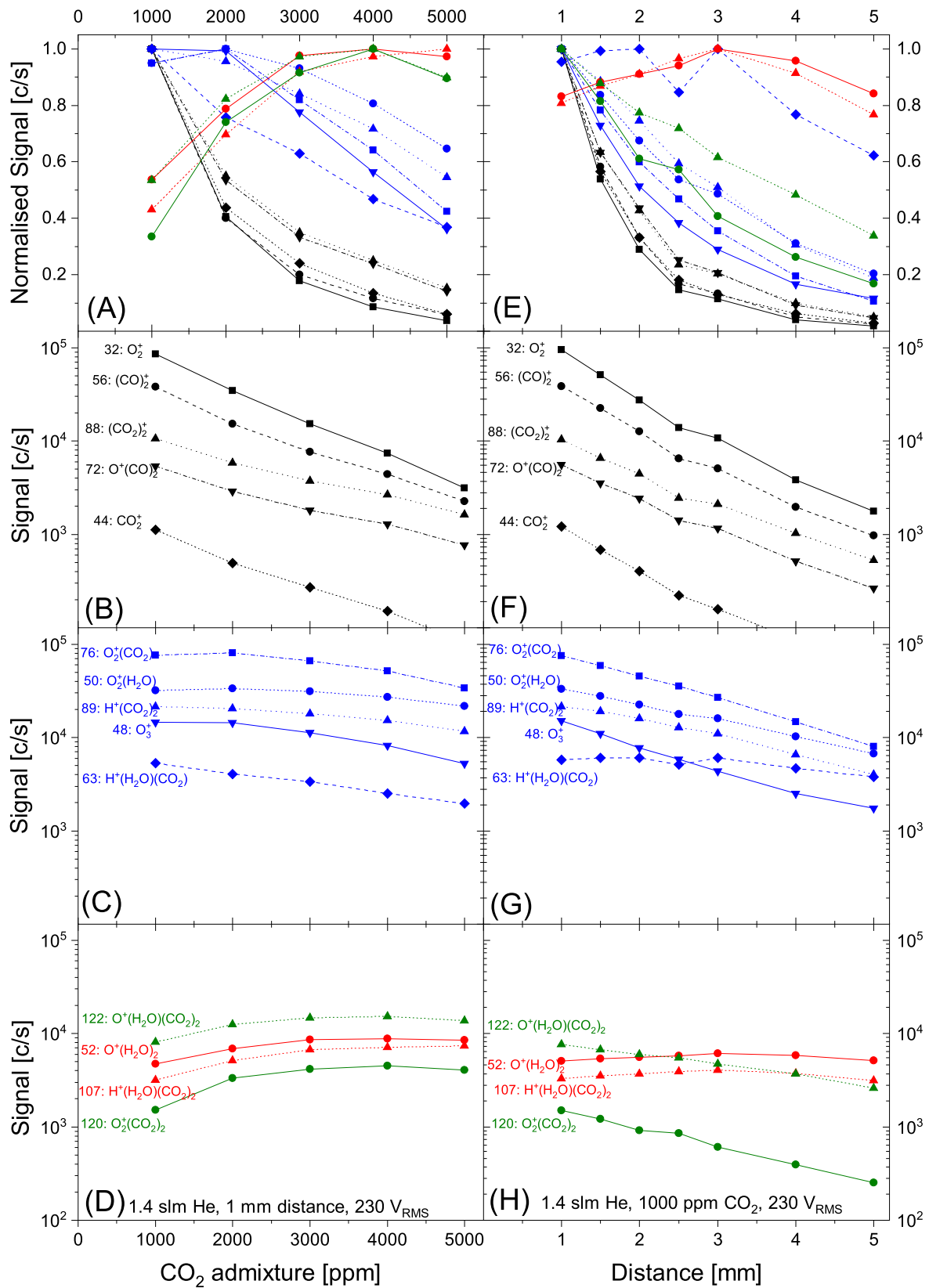
Figure 10 shows the ion spectrum for a 1000 ppm CO<sub>2</sub> admixture at 1 mm distance and 230 V<sub>RMS</sub> applied voltage. A very strong signal of O<sub>2</sub><sup>+</sup> is visible as well as a strong signal for O<sub>3</sub><sup>+</sup>, O<sub>2</sub><sup>+</sup>(H<sub>2</sub>O), C<sub>2</sub>O<sub>2</sub><sup>+</sup> and O<sub>2</sub><sup>+</sup>(CO<sub>2</sub>). O<sub>2</sub> has the lowest ionisation energy from the observed primary ions (12.07 eV, water molecule has for comparison ionisation energy of 12.62 eV), explaining its dominance in the spectrum. Further, there are several H<sub>2</sub>O clusters visible such as H<sup>+</sup>(H<sub>2</sub>O)<sub>2</sub>, O<sub>2</sub><sup>+</sup>(H<sub>2</sub>O), H<sup>+</sup>(H<sub>2</sub>O)(CO<sub>2</sub>) and O<sup>+</sup>(H<sub>2</sub>O)(CO<sub>2</sub>)<sub>2</sub>.

Only relative signal intensities, but no absolute ion densities, have been measured. Nevertheless, the ion densities are estimated to be at maximum  $1 \times 10^8 \text{ cm}^{-3}$ , based on a simulation of the transfer function for this mass spectrometer [36]. This estimation supports the expectation that the ion densities in the effluent are much lower compared to the plasma density ( $n_e \approx 10^{11} \text{ cm}^{-3}$  [26]), due to the fast recombination of ions with other ions ( $k \approx 10^{-7} \text{ cm}^3 \text{ s}^{-1}$ ) [53]. Therefore, the ions play an insignificant role in the recombination chemistry in the plasma effluent of this remote plasma jet.

An admixture and a distance variation was conducted and is presented in figure 11. Generally four groups of ions can be distinguished when the signal is normalised (on the maximum of each species), see figures 11(A) and (E). The division of ions into groups is given in table 2.

First the general trend is discussed. The first group (black) shows an exponential decay with increasing admixture (figure 11(A)) and increasing distance (figure 11(E)). For the second group (blue) no decrease is present up to 2000 ppm admixture, afterwards a near-linear decrease is observed. This group shows a slower exponential decay with

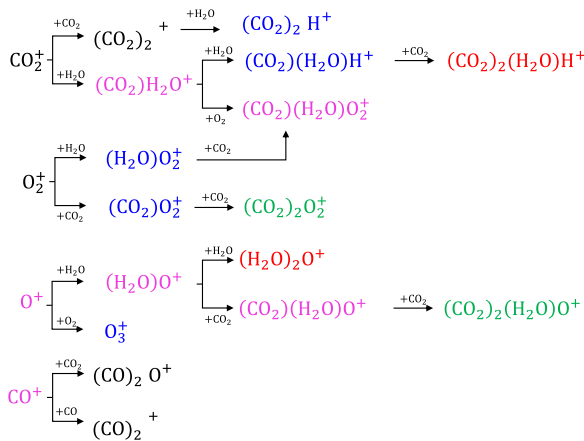




**Figure 11.** Influence of admixture and distance variation on selected ions in the plasma effluent in a He/CO<sub>2</sub> gas mixture. When the measured signal is normalised (A), (E), four different groups can be distinguished. These are detailed in (B)–(D) and (F)–(H) and in table 2. The statistical error for all signals is smaller than 5%. Due to the logarithmic scale the error bars are within the size of the symbol.

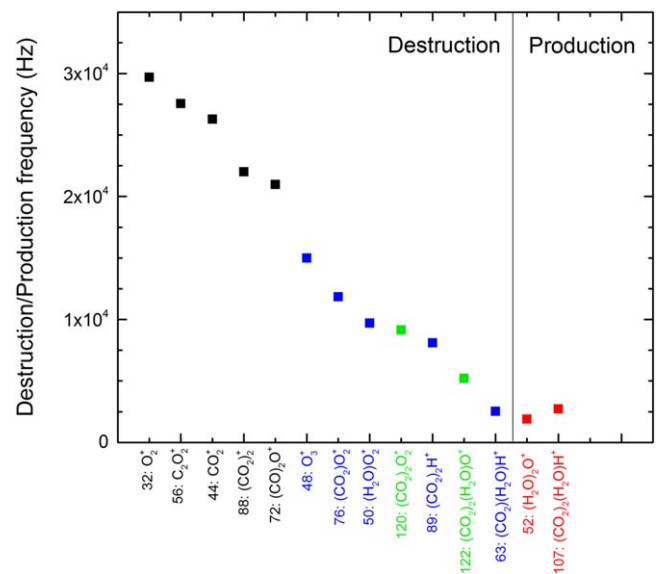
**Table 2.** List of all measured ions in the plasma effluent in a He/CO<sub>2</sub> gas mixture. Four different groups can be distinguished in figure 11. The ions between straight brackets [] are not included in this figure.

Group 1 (Black)		Group 2 (Blue)		Group 3 (Red)	
Ion	Mass	Ion	Mass	Ion	Mass
[H <sup>+</sup> (H <sub>2</sub> O)]	19	[H <sup>+</sup> (H <sub>2</sub> O) <sub>2</sub> ]	37	O <sup>+</sup> (H <sub>2</sub> O) <sub>2</sub>	52
O <sub>2</sub> <sup>+</sup>	32	O <sub>3</sub> <sup>+</sup>	48	H <sup>+</sup> (H <sub>2</sub> O)(CO <sub>2</sub> ) <sub>2</sub>	107
[O <sup>+</sup> (H <sub>2</sub> O)]	34	O <sub>2</sub> <sup>+</sup> (H <sub>2</sub> O)	50		
CO <sub>2</sub> <sup>+</sup>	44	H <sup>+</sup> (H <sub>2</sub> O)(CO <sub>2</sub> )	63		
(CO) <sub>2</sub> <sup>+</sup>	56	O <sub>2</sub> <sup>+</sup> (CO <sub>2</sub> )	76		
O <sup>+</sup> (CO) <sub>2</sub>	72	H <sup>+</sup> (CO <sub>2</sub> ) <sub>2</sub>	89		
(CO <sub>2</sub> ) <sub>2</sub> <sup>+</sup>	88				
				<b>Group 4 (Green)</b>	
				O <sub>2</sub> <sup>+</sup> (CO <sub>2</sub> ) <sub>2</sub>	120
				O <sup>+</sup> (H <sub>2</sub> O)(CO <sub>2</sub> ) <sub>2</sub>	122

**Figure 12.** Example of cluster formation in the plasma effluent in a He/CO<sub>2</sub> gas mixture. Starting from the primary ions CO<sub>2</sub><sup>+</sup>, O<sub>2</sub><sup>+</sup>, O<sup>+</sup>, and CO<sup>+</sup>, water or CO<sub>2</sub> clusters are formed as this is energetically favourable. The observed clusters are colour coded as in figure 11, clusters in magenta colour have too low intensity and are visible only in log scale.

increasing distance compared to the black group. The third (red) and fourth (green) group show an initial increase with increasing admixture followed by a saturation starting from 3000 ppm. Whereas the fourth group shows a linear decrease with increasing distance, the third group increases until a maximum is reached at about 3 mm, after which the signal decreases again.

The dependence of each group on admixture is shown in figures 11(B)–(D) and the dependence on distance in figures 11(F)–(H). Generally, a similar trend of increase of the cluster size has been observed in case of increasing the distance from the jet, and in case of increasing the CO<sub>2</sub> admixture. The smaller or primary ions (group 1—figure B and F) react to build medium clusters (group 2—figure C and G), which then build larger clusters (group 3 and 4—figure D and G). The process of cluster building explains the observed trends, as the probability of building a clusters increases when more CO<sub>2</sub> is admixed or when the distance, i.e. reaction time in the effluent, is increased. The clustering process is given in figure 12 starting with smaller or primary ions (group 1) building medium clusters (group 2), eventually leading larger cluster with H<sub>2</sub>O and CO<sub>2</sub> molecules (group 3 and 4). The trend of group 4 containing CO<sub>2</sub> and oxygen ions exhibits

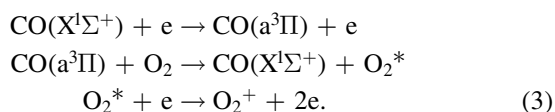
**Figure 13.** Destruction and production frequencies of selected ions (as a function of distance) as determined in the first 3 mm distance from the jet nozzle with gas velocity of 20 m s<sup>-1</sup>.

production trend with CO<sub>2</sub> admixture addition and destruction trend with the increase of distance. As molecules in group 4 are CO<sub>2</sub> and oxygen ion rich, higher CO<sub>2</sub> admixture will support creation of such cluster, while increasing the distance at a given admixture will result in destruction behaviour similar to the ion clusters in group 2, as shown in figure 11(E) and in figure 13.

The trend of high loss frequency of the small molecules (Group 1) due to clustering can be clearly visualised as a plot of the loss frequency for different group of ions, as shown in figure 13. The medium size clusters (Group 2) have lower loss frequency, while Group 3 ions exhibit a production trend. The destruction/production frequency has been calculated for the first 3 mm from each ion exponential decay assuming gas velocity of 20 m s<sup>-1</sup> (1.4 slm gas flow through 1 mm<sup>2</sup> cross section of the jet). The decay of CO<sub>2</sub> related ions due to collisions with H<sub>2</sub>O and O<sub>2</sub> has been studied and reported by Ikezoe *et al* [49].

It is remarkable that no CO<sup>+</sup> ions are detected in the plasma effluent. This is likely due to charge exchange processes as well as the reactions (3), leading to the strong signal of O<sub>2</sub><sup>+</sup> [48]. The formation of clusters based on O<sub>2</sub><sup>+</sup>, explains

the strong signal of  $O_2^+(CO_2)$  and  $O_2^+(H_2O)$ . It should be noted that  $He^+$  and also  $He_2^+$  are not formed in the helium gas mixture with some additional gas admixture due to very high helium ionisation energy of 24.59 eV (see for example the global model results of Liu *et al* for He/ $O_2$  plasma [54])



## Conclusions

The neutral species CO, O,  $O_2$  and  $O_3$  as well as various positive ions were observed when admixing  $CO_2$  into the helium feed gas of radio frequency driven the atmospheric pressure plasma (predecessor of the COST reference jet with identical performance). During experiments the  $CO_2$  admixture, applied voltage and distance were varied.

Absolutely calibrated densities were obtained for the neutral species. The density of all neutral species, except ozone, was in the range of  $10^{14}$  to  $10^{15} \text{ cm}^{-3}$ . The ozone density was in the range of  $10^{12}$ – $10^{13} \text{ cm}^{-3}$ . Notable is the very high atomic oxygen density (18 ppm O) relative to the molecular oxygen density (13 ppm  $O_2$ ). The very low reaction rates of atomic oxygen with ground state  $CO_2$  and CO are very probably responsible for this high O density and it could indicate that vibrational excitation of  $CO_2$  is not effective in this discharge and gas mixture.

An analysis of the neutral reaction chemistry was conducted based on reaction rates available in literature. Most trends can be explained based on this analysis. An exception is the small decrease of CO density in the first millimetres of the effluent, which could not be explained. The measured absolute densities of  $O_2$ , O, and  $O_3$  add up to the 57% of the oxygen balance of the  $CO_2$  dissociation. It is not clear at the moment, whether the remaining deficiency of the gas mixture in oxygen is due to loss of oxygen in reactions with gas impurities (mainly  $N_2$ ,  $H_2O$  leading to  $NO_x$  or  $H_2O_2$  species), surface reactions or due to possible systematic error in the density calibration.

The conversion efficiency of  $CO_2$  into CO is the largest (~13%) at admixtures below 500 ppm (energy efficiency is below 1%). The energy efficiency is the largest (~5%) at high  $CO_2$  admixtures, where the conversion efficiency is only around one percent or below. These low values of conversion and energy efficiencies are expected for this type of cold highly diluted  $CO_2$  plasma operated at low power in the diffuse mode. The results are similar to performance of dielectric barrier discharges.

A large number of ions and ion clusters were observed.  $O_2^+$  is dominant in the ion spectrum and as direct consequence most ion clusters are  $O_2^+$  based  $[O_2^+(H_2O)_x(CO_2)_y]$ . No  $CO^+$  ion was observed, which is likely due to charge transfer reactions favouring  $O_2^+$ . The ion chemistry follows the known transformation of primary ions




into secondary ions and terminal ions, i.e. ions in which the charge transfer chain terminates. This is based on an initial analysis, as a detailed analysis of the ion chemistry by an extended reaction rate model is not pursued here.

The obtained result can serve as a test bed of current plasma-chemistry models used for the study of the  $CO_2$  conversion processes.

## Acknowledgments

This project has received funding from the Seventh Framework Programme for research, technological development and demonstration of the European Union under the grant agreement no. 606889 Marie Curie ITN RAPID (Reactive Atmospheric Plasma processIng-eDucation network), the Cooperative Research Centre CRC 1316 (Transient Atmospheric Pressure Plasmas: from plasmas to liquids to solids) and the project BE 4349/5-1 of the German Research Foundation. All support is gratefully acknowledged.

## ORCID iDs

Ante Hecimovic  <https://orcid.org/0000-0002-3281-8507>  
Emile Carbone  <https://orcid.org/0000-0003-3455-0708>  
Jan Benedikt  <https://orcid.org/0000-0002-8954-1908>

## References

- [1] Snoeckx R and Bogaerts A 2017 Plasma technology—a novel solution for  $CO_2$  conversion? *Chem. Soc. Rev.* **46** 5805–63
- [2] Fridman A 2012 *Plasma Chemistry* (Cambridge: Cambridge University Press)
- [3] Capitelli M *et al* 2017 Self-consistent time dependent vibrational and free electron kinetics for  $CO_2$  dissociation and ionization in cold plasmas *Plasma Sources Sci. Technol.* **26** 055009
- [4] Silva T *et al* 2018 Modelling the input and relaxation of vibrational energy in  $CO_2$  plasmas *J. Phys. D: Appl. Phys.* **51** 464001
- [5] Silva T *et al* 2018 Kinetic study of low-temperature  $CO_2$  plasmas under non-equilibrium conditions: I. Relaxation of vibrational energy *Plasma Sources Sci. Technol.* **27** 015019
- [6] Armenise I and Kustova E V 2013 State-to-state models for  $CO_2$  molecules: from the theory to an application to hypersonic boundary layers *Chem. Phys.* **415** 269–81
- [7] Berthelot A and Bogaerts A 2016 Modeling of plasma-based  $CO_2$  conversion: lumping of the vibrational levels *Plasma Sources Sci. Technol.* **25** 045022
- [8] Koelman P *et al* 2017 A comprehensive chemical model for the splitting of  $CO_2$  in non-equilibrium plasmas *Plasma Process. Polym.* **14** 1600155
- [9] Wang W and Bogaerts A 2016 Effective ionisation coefficients and critical breakdown electric field of  $CO_2$  at elevated temperature: effect of excited states and ion kinetics *Plasma Sources Sci. Technol.* **25** 055025
- [10] Berthelot A and Bogaerts A 2017 Modeling of  $CO_2$  plasma: effect of uncertainties in the plasma chemistry *Plasma Sources Sci. Technol.* **26** 115002

- [11] Kozák T and Bogaerts A 2014 Splitting of CO<sub>2</sub> by vibrational excitation in nonequilibrium plasmas: a reaction kinetics model *Plasma Sources Sci. Technol.* **23** 045004
- [12] Bogaerts A *et al* 2015 Plasma-based conversion of CO<sub>2</sub>: current status and future challenges *Faraday Discuss.* **183** 217–32
- [13] Aerts R, Martens T and Bogaerts A 2012 Influence of vibrational states on CO<sub>2</sub> splitting by dielectric barrier discharges *J. Phys. Chem. C* **116** 23257–73
- [14] Aerts R, Somers W and Bogaerts A 2015 Carbon dioxide splitting in a dielectric barrier discharge plasma: a combined experimental and computational study *ChemSusChem* **8** 702–16
- [15] Kozák T and Bogaerts A 2014 Evaluation of the energy efficiency of CO<sub>2</sub> conversion in microwave discharges using a reaction kinetics model *Plasma Sources Sci. Technol.* **24** 015024
- [16] Heijkens S *et al* 2015 CO<sub>2</sub> conversion in a microwave plasma reactor in the presence of N<sub>2</sub>: elucidating the role of vibrational levels *J. Phys. Chem. C* **119** 12815–28
- [17] Bogaerts A *et al* 2016 Modeling plasma-based CO<sub>2</sub> conversion: crucial role of the dissociation cross section *Plasma Sources Sci. Technol.* **25** 055016
- [18] Heijkens S *et al* 2019 Nanosecond pulsed discharge for CO<sub>2</sub> conversion: kinetic modeling to elucidate the chemistry and improve the performance *J. Phys. Chem. C* **123** 12104–16
- [19] Wang W *et al* 2016 CO<sub>2</sub> conversion in a gliding arc plasma: 1D cylindrical discharge model *Plasma Sources Sci. Technol.* **25** 065012
- [20] van Dijk J *et al* 2009 The plasma modelling toolkit Plasimo *J. Phys. D: Appl. Phys.* **42** 194012
- [21] Graves D B 2017 Mechanisms of plasma medicine: coupling plasma physics, biochemistry, and biology *IEEE Trans. Radiat. Plasma Med. Sci.* **1** 281–92
- [22] Carbone E and Douat C 2018 Carbon monoxide in plasma medicine and agriculture: just a foe or a potential friend? *Plasma Med.* **1** 93
- [23] Jeong J Y *et al* 1998 Etching materials with an atmospheric-pressure plasma jet *Plasma Sources Sci. Technol.* **7** 282–5
- [24] Schütze A *et al* 1998 The atmospheric-pressure plasma jet: a review and comparison to other plasma sources *IEEE Trans. Plasma Sci.* **26** 1685–94
- [25] Golda J *et al* 2016 Concepts and characteristics of the ‘COST reference microplasma jet’ *J. Phys. D: Appl. Phys.* **49** 084003
- [26] Waskoenig J *et al* 2010 Atomic oxygen formation in a radio-frequency driven micro atmospheric pressure plasma jet *Plasma Sources Sci. Technol.* **19** 045018
- [27] Willems G *et al* 2019 Corrigendum: Characterization of the effluent of a He/O<sub>2</sub> micro-scaled atmospheric pressure plasma jet by quantitative molecular beam mass spectrometry *New J. Phys.* **21** 059501
- [28] Willems G *et al* 2010 *New J. Phys.* **12** 013021
- [29] Willems G, Benedikt J and von Keudell A 2017 Absolutely calibrated mass spectrometry measurement of reactive and stable plasma chemistry products in the effluent of a He/H<sub>2</sub>O atmospheric plasma *J. Phys. D: Appl. Phys.* **50** 335204
- [30] Benedikt J, Ellerweg D and von Keudell A 2009 Molecular beam sampling system with very high beam-to-background ratio: the rotating skimmer concept *Rev. Sci. Instrum.* **80** 055107
- [31] Benedikt J *et al* 2013 Mass spectrometry of positive ions and neutral species in the effluent of an atmospheric pressure plasma with hexamethyldisiloxane and oxygen *J. Phys. D: Appl. Phys.* **46** 464017
- [32] Ellerweg D 2012 Reaction chemistry in oxygen or hexamethyldisiloxane containing noble gas microplasma jets: a quantitative molecular beam mass spectrometry study *PhD Thesis* Bochum: Ruhr-University Bochum
- [33] Hefny M M *et al* 2019 The transport and surface reactivity of O atoms during the atmospheric plasma etching of hydrogenated amorphous carbon films *Plasma Sources Sci. Technol.* **28** 035010
- [34] Knuth E L 1995 Composition distortion in MBMS sampling *Combust. Flame* **103** 171–80
- [35] McCay T D and Linwood L 1983 Diffusive separation of binary mixtures of CO<sub>2</sub>–H<sub>2</sub> in a sonic-orifice expansion *Phys. Fluids* **26** 2115
- [36] Ellerweg D *et al* 2010 Characterization of the effluent of a He/O<sub>2</sub> microscale atmospheric pressure plasma jet by quantitative molecular beam mass spectrometry *New J. Phys.* **12** 013021
- [37] Große-Kreul S 2015 Mass spectrometry of ions from atmospheric pressure plasmas *PhD Thesis* Bochum: Ruhr-University Bochum
- [38] Große-Kreul S *et al* 2016 Sampling of ions at atmospheric pressure: ion transmission and ion energy studied by simulation and experiment *Eur. Phys. J. D* **70** 103
- [39] Tsang W and Hampson R F 1986 Chemical kinetic data base for combustion chemistry: I. Methane and related compounds *J. Phys. Chem. Ref. Data* **15** 1087–279
- [40] Hippler H, Rahn R and Troe J 1990 Temperature and pressure dependence of ozone formation rates in the range 1–1000 bar and 90–370 K *J. Chem. Phys.* **93** 6560
- [41] IUPAC Task Group on Atmospheric Chemical Kinetic Data Evaluation <http://iupac.pole-ether.fr/>
- [42] NIST Chemical Kinetics Database [kinetics.nist.gov](http://kinetics.nist.gov)
- [43] Berthelot A 2017 private communication
- [44] van den Bekerom D C M *et al* 2019 The importance of thermal dissociation in CO<sub>2</sub> microwave discharges investigated by power pulsing and rotational Raman scattering *Plasma Sources Sci. Technol.* **28** 055015
- [45] Savinov S Y *et al* 1999 Decomposition of methane and carbon dioxide in a radio-frequency discharge *Ind. Eng. Chem. Res.* **38** 2540–7
- [46] Savinov S Y *et al* 2002 The decomposition of CO<sub>2</sub> in glow discharge *Korean J. Chem. Eng.* **19** 564–6
- [47] Spencer L F and Gallimore A D 2010 Efficiency of CO<sub>2</sub> dissociation in a radio-frequency discharge *Plasma Chem. Plasma Process.* **31** 79–89
- [48] Urbanietz T *et al* 2018 Non-equilibrium excitation of CO<sub>2</sub> in an atmospheric pressure helium plasma jet *J. Phys. D: Appl. Phys.* **51** 345202
- [49] Kaufman Y *et al* 1980 Ion clusters in He/CO and Ar/CO glow discharges *J. Chem. Phys.* **72** 2606–11
- [50] Ikezoe Y *et al* 1982 Ions in carbon dioxide at an atmospheric pressure *Radiat. Phys. Chem.* **20** 253
- [51] Große-Kreul S *et al* 2015 Mass spectrometry of atmospheric pressure plasmas *Plasma Sources Sci. Technol.* **24** 044008
- [52] Oh J-S, Aranda-Gonzalvo Y and Bradley J W 2011 Time-resolved mass spectroscopic studies of an atmospheric-pressure helium microplasma jet *J. Phys. D: Appl. Phys.* **44** 365202
- [53] Große-Kreul S *et al* 2016 Methods of gas purification and effect on the ion composition in an RF atmospheric pressure plasma jet investigated by mass spectrometry *EPJ Techniq. Instrum.* **3** 322
- [54] Hickman A 1979 Approximate scaling formula for ion–ion mutual neutralization rates *J. Chem. Phys.* **70** 4872
- [55] Liu D-X *et al* 2010 Main species and physicochemical processes in cold atmospheric-pressure He + O<sub>2</sub> plasmas *Plasma Process. Polym.* **7** 846